REPORT DOCUMENTATION PAGE

Form Approved OMB No. 0704-0188

1. REPORT DATE *(DD-MM-YYYY)*	2. REPORT TYPE	3. DATES COVERED *(From - To)*
	Technical Papers	

4. TITLE AND SUBTITLE

5a. CONTRACT NUMBER

5b. GRANT NUMBER

5c. PROGRAM ELEMENT NUMBER

6. AUTHOR(S)

5d. PROJECT NUMBER
2303

5e. TASK NUMBER
M2C8

5f. WORK UNIT NUMBER

7. PERFORMING ORGANIZATION NAME(S) AND ADDRESS(ES)

Air Force Research Laboratory (AFMC)
AFRL/PRS
5 Pollux Drive
Edwards AFB CA 93524-7048

8. PERFORMING ORGANIZATION REPORT

9. SPONSORING / MONITORING AGENCY NAME(S) AND ADDRESS(ES)

Air Force Research Laboratory (AFMC)
AFRL/PRS
5 Pollux Drive
Edwards AFB CA 93524-7048

10. SPONSOR/MONITOR'S ACRONYM(S)

11. SPONSOR/MONITOR'S NUMBER(S)

12. DISTRIBUTION / AVAILABILITY STATEMENT

Approved for public release; distribution unlimited.

13. SUPPLEMENTARY NOTES

14. ABSTRACT

15. SUBJECT TERMS

16. SECURITY CLASSIFICATION OF:			17. LIMITATION OF ABSTRACT	18. NUMBER OF PAGES	19a. NAME OF RESPONSIBLE PERSON
a. REPORT	b. ABSTRACT	c. THIS PAGE			Leilani Richardson
Unclassified	Unclassified	Unclassified	A		19b. TELEPHONE NUMBER *(include area code)* (661) 275-5015

62 separate items are enclosed

TP-1998-168

MEMORANDUM FOR IN-HOUSE PUBLICATIONS

30 Sep 98

FROM: PROI (TI) (STINFO)

SUBJECT: Authorization for Release of Technical Information, Control Number: AFRL-PR-ED-TP-1998-168
S. Tam and M.E. Fajardo "An Ortho/para Hydrogen Converter for Rapid Deposition Matrix Isolation Spectroscropy

Public Release Review **(Statement A)**

An ortho/para Hydrogen Converter for Rapid Deposition Matrix Isolation Spectroscopy

Simon Tam and Mario E. Fajardo[a)]

Propulsion Directorate, US Air Force Research Laboratory

AFRL/PRSP, Bldg. 8451, Edwards AFB, CA 93524-7680

[a)] email: Mario_Fajardo@ple.af.mil

Submitted to Rev. Sci. Instr. _____, Received _____, Accepted _____

ABSTRACT

We describe the construction and operation of a catalyst-bed type device for precooling and equilibrating the ortho/para composition of a hydrogen gas flow. We use this device to vapor deposit millimeters thick cryogenic parahydrogen (pH_2) solids which are remarkably transparent [M.E. Fajardo and S. Tam, J. Chem. Phys. **108**, 4237 (1998)]. Infrared absorption spectra of solids deposited at pH_2 flow rates up to 290 mmol/hour (solid thickness growth rates up to 75 μm/min) indicate a residual orthohydrogen (oH_2) content of less than 0.01%. Gas phase thermal conductivity measurements indicate a residual oH_2 content of $0(^{+5}_{-0})$% for flow rates up to 1.9 mol/hour. These pH_2 solids can be doped readily by simple co-deposition of various impurities produced by any of the numerous dopant sources developed in previous matrix isolation spectroscopy (MIS) studies. The long achievable pathlengths, and the desirable properties of pH_2 as a matrix host, will enable revolutionary new fundamental and practical applications for MIS.

I. INTRODUCTION

A. Matrix Isolation Spectroscopy

In matrix isolation spectroscopy (MIS), chemical dopant species are trapped in a solid host environment for spectroscopic study.[1-4] MIS studies have contributed to the general body of scientific knowledge in several ways. They have characterized the structures and spectroscopic properties of numerous previously unknown chemical species, including free radicals and transient reactive intermediates, guiding the way for gas-phase spectroscopic efforts and yielding new insights into chemical reaction mechanisms. They have demonstrated the synthesis of novel chemical compounds by combining the extremes of temperature: condensation of "high temperature" species such as metal vapors along with other reactants in a cryogenic solid. They have provided model systems for understanding spectroscopy and reactive dynamics in more complex condensed phase systems; the high number densities and low temperatures achieved in a matrix enhance the roles of many-body interactions and "quantum" effects, for example. From a practical viewpoint, the matrix serves as a long time integrating detector in which chemical species can be collected by deposition, or built up in-situ, to readily detectable levels. Hence, MIS techniques have been employed advantageously in analytical and diagnostic applications.

Many materials can serve as matrix hosts, however the majority of MIS studies have been performed in cryogenic van der Waals solids including: Ne, Ar, Kr, Xe, N_2, CO, O_2, CO_2, CH_4, and SF_6. Traditionally, these solids are formed by in-vacuum co-deposition of the matrix host and dopant (or dopant precursor(s)) onto a flat cryogenic substrate, although other deposition geometries have seen use. Factors influencing the choice of dopant/host combinations include: spectral compatibility, chemical reactivity, dopant isolation efficiency, and stringency of cryogenic requirements for achieving thermally stable low vapor pressure samples. Despite past neglect, recently the solid molecular hydrogens[5] (SMH; i.e. H_2 and its isotopomers) have enjoyed increasing popularity as matrix hosts. We hope to contribute to this trend by showing that, in many cases, the desirable properties of the SMH as matrix hosts far outweigh the difficulties associated with their use, and that these difficulties can be overcome by using the invention described in this manuscript.

B. Solid Molecular Hydrogens as Matrix Hosts

Although incapable of matching the chemical inertness of the rare gases (Rg), the SMH should be serviceable hosts for dopants with which reactions are endothermic or exhibit even a modest activation barrier. We have previously surveyed the field of trapping of light atomic dopants in SHM,[6] as part of our ongoing efforts within the US Air Force's High Energy Density Matter (HEDM) program to determine the feasibility of utilizing such systems as advanced chemical propellants.[7] To date, good experimental evidence exists for the isolation of chemically distinct H, Li, B, N, O, Na, Mg, Al, and other heavier and/or inert atoms in SMH. Although few in comparison to studies in Rg, MIS studies of stable molecules in SMH date back at least 25 years,[8] and photolysis of molecules trapped in SMH[9] has recently been employed to produce molecular radical species trapped in SMH.[10] Thus, a variety of spectroscopically and chemically interesting dopants show sufficient chemical compatibility to be trapped in SMH.

The SMH were once considered to be "quite unusable" as matrix hosts "because they do not form rigid solids and have high vapor pressures even at 4 K."[ref. 2] The vapor pressure problem can be overcome readily in a liquid helium (lHe) bath cryostat by pumping on the lHe cryogen to produce deposition substrate temperatures of $\approx$ 2 K. We have been able to deposit doped 1-10 μm thick films of normal-H_2 (nH_2, ref. 11) at substrate temperatures as high as 3.5(±0.5) K, and normal-D_2 at 4.5(±0.5) K; at these temperatures the vapor pressures are of order 10^{-8} to 10^{-9} Torr [ref. 12]. The issue of host rigidity pertains to the dopant isolation efficiency and the capacity for long-term storage of trapped species. The empirical evidence listed in the previous paragraph demonstrates that the SMH are sufficiently "rigid" for MIS purposes, although working at the lowest achievable temperatures in a given experimental apparatus is recommended for minimizing dopant mobility and recombination.

The SMH have both desirable and objectionable optical properties as MIS hosts. There exist several broad and useful infrared (IR) and visible transmission windows between the various condensed phase induced rotational-vibrational absorptions[13-15] and their overtones.[16] As wide bandgap dielectrics, the SMH are essentially transparent throughout the visible (vis) and ultraviolet (UV) spectral regions, with the onset of excitonic absorptions[17] occurring near 110 nm ($\approx$ 11 eV), well into the vacuum UV region. An exciting recent development is the demonstration that solid parahydrogen[11] (pH_2) is compatible with high resolution ($\Delta\nu/\nu < 10^{-6}$) IR

absorption and nonlinear optical spectroscopies[18-21] of both dopant molecules and the pH_2 host; the "quantum solid" nature and "softness" of the pH_2 host (properties once considered detrimental for MIS!) are cited as contributing to this phenomenon. Future application of high resolution spectroscopic techniques in doped pH_2 solids holds the promise of a deeper and more quantitative understanding of their microscopic structure and dynamics than has been achieved via MIS for Rg host matrices.

The major practical difficulty in using the SMH as MIS hosts has been the strong optical scattering properties of vapor deposited hydrogen solids,[22] particularly those produced in the traditional MIS substrate-in-vacuum geometry.

> "Good crystals are always grown slowly from the melt; a rapid freeze from the gas produces snow... a 1 mm-thick layer of hydrogen crystallites can be a completely opaque brown-black." [ref. 22]

Such samples are likely polycrystalline with microcrystallites having dimensions comparable to optical wavelengths; the optical scattering resulting from abrupt changes in the refractive index at the numerous microcrystallite boundaries.[22] Optical scattering losses in the UV region of 80 to 90% are typically encountered in vapor deposited nH_2 films only 10 μm thick. Absorption spectra of dopant species obtained from such matrices suffer from poor signal-to-noise ratios, and from lineshape distortion during the numerical wavelength dependent baseline correction process. Such optical scattering losses limit SMH matrix thicknesses to ~ 10 μm for work in the UV/vis, and ~ 100 μm for IR absorption spectra. While these thicknesses are adequate for many MIS applications, they do not allow for spectroscopic characterization of the SMH host itself, or of dopants with either low concentrations or inherently weak absorptions.

One successful approach to overcoming the optical scattering problem and obtaining very long optical pathlengths has been to prepare pH_2 solids by gas condensation within an enclosed cell held at ≈ 0.5 of the pH_2 triple point temperature[18-21] ($T_{tp}(pH_2) = 13.8$ K; T_{cell} is typically 7 to 8 K). Transparent doped and pure pH_2 solids up to 11.5 cm thick have been prepared in this manner and characterized spectroscopically.[18] Similar techniques for condensing other matrix host gases in semi-enclosed cells also produce large transparent solids.[23-26] Unfortunately,

deposition at temperatures above $\approx 0.3\ T_{tp}$ requires that dopant concentrations be kept well below $\approx$ 100 PPM to avoid extensive aggregation and clustering. Additionally, sample preparation by condensation in an enclosed cell is not compatible with many extant dopant introduction schemes developed for substrate-in-vacuum depositions. Despite these limitations, the pioneering work which demonstrated high-resolution spectroscopy in pH_2 solids was performed on such cell-grown samples. Thus, these samples stand as the benchmark against which the product of any new sample preparation technique must be measured.

C. Rapid Deposition Matrix Isolation Spectroscopy

We have developed an alternative doped solid pH_2 preparation technique. We recently reported the production of optically transparent millimeters-thick (pH_2) solids by rapid in-vacuum deposition of pre-cooled pH_2 gas, and the doping of those solids with various atomic and molecular, neutral and charged species.[27] We note that our efforts to produce gram-scale pH_2 solids were driven by the technological requirement of scaling up HEDM sample production while retaining the desirable aspects of the in-vacuum deposition method for introducing energetic dopants (simplicity, versatility, etc.). We had also considered the possibility that depositing pre-cooled pH_2 gas, instead of room temperature nH_2 gas, would greatly reduce the heat load on the matrix accretion layer and eliminate internal heat production due to ortho-para conversion in the solid, thereby inhibiting the recombination of our energetic dopants. We found, serendipitously, that the diminished deposition heat load rate allows us to utilize pre-cooled pH_2 gas flow rates hundreds of times faster than typically employed in conventional MIS experiments, and that the resulting pH_2 solids are so transparent as to escape detection by casual visual inspection! We speculate that these high deposition rates somehow allow for "self-annealing" of the accreting surface of the matrix during deposition, resulting in larger and fewer crystallites, and hence in greatly reduced optical scattering.

We predicted in our preliminary report[27] that this new deposition technique will result in a pronounced improvement in the quality and types of spectroscopic information obtainable from MIS experiments. Quantitatively, the millimeters long useful optical pathlengths yield an obvious advantage in the detection of low concentration or weakly absorbing dopants over the typically much thinner Rg matrices. The applicability of high resolution spectroscopic

techniques also promises important analytical advantages in detecting and identifying trapped species.

Not so obvious is the qualitatively different type of information contained within the induced IR activity of the pH_2 host itself. Whereas Rg hosts are essentially silent perturbers of the spectroscopic properties of trapped dopants, the response of the pH_2 host to the presence of dopants is directly observable.[27] Furthermore, the complexity of the pattern of induced IR activity in the pH_2 host appears to increase within the dopant sequence: atom, diatomic, polyatomic. Our preliminary interpretation is that this increased complexity reflects the greater variety of distinct chemical environments for the nearest neighbor pH_2 molecules. Thus, a single IR absorption spectrum of doped solid pH_2 explicitly contains information about both the "solutes" and the "solvent."

In what follows we describe the construction, operation, and performance of our ortho/para hydrogen converter (o/p converter), presenting our techniques in sufficient detail to facilitate their adoption and improvement by the interested reader. We characterize the performance of the o/p converter by two different techniques: IR absorption of H_2 solids deposited at flow rates up to 300 mmol/hour, and gas phase thermal conductivity (TC) measurements on H_2 gas samples collected using flow rates over 1 mol/hr. The IR absorption diagnostic is the most sensitive to the presence of oH_2 molecules, but is limited to slower H_2 flow rates than the TC technique. One caveat: while our implementation of the transient hot-wire TC method was adequate to the task at hand, we've left considerable room for improvement, and direct the interested reader to the original literature in this field.

II. EXPERIMENTAL

A. Construction of o/p Converter

Figure 1 shows the oxygen free high conductivity (OFHC) copper bobbin which forms the core of our o/p converter. The bobbin supports a 3.2 mm outside diameter (OD) by 1.5 m long piece of copper refrigeration tubing packed with 1.4 g of APACHI catalyst (a paramagnetic nickel salt supported on particulate silica gel[5]). Pyrex glass wool pushed into both ends of the copper tube holds the catalyst particles in place. The tube is wound around the bobbin in three layers; the hole labeled "gas line out" and the slot labeled "gas line in" in figure 1 imply the

winding direction. The gas outlet end of the tube protrudes through the center of the circular face of the bobbin and terminates in a modified brass compression fitting (not shown) which was silver soldered to the tube prior to packing of the catalyst. This fitting facilitates connection of the output of the o/p converter to the various sample preparation and testing apparatus.

The tubing is potted onto the bobbin with a silver-powder-filled thermally conductive epoxy. Prior to winding, both the bobbin and the outside of the tube were chemically cleaned with a "bright dip" mixed acids solution.[28] Generous application of the epoxy during the winding process helps eliminate voids. The epoxy is cured by heating the entire bobbin/tube assembly (catalyst open to air) in an oven at 150 °C for 6 hours.

The catalyst must be initially activated by heating to remove contaminant "poisons" [ref. 5]. We connect the inlet end to a gas handling manifold, and the outlet end to a high vacuum chamber equipped with a residual gas analyzer (RGA). Heating the bobbin/tube assembly to 165 °C with the inlet valve closed results in the evolution of water and other atmospheric gases. After an hour we begin a slow flow of H_2 gas which reduces the O_2 and increases the H_2O levels detected by the RGA. After another two hours the bobbin/tube assembly is allowed to cool to room temperature, then vented to dry Ar gas in preparation for transfer and incorporation into the o/p converter.

The bobbin/tube assembly is mounted in a vacuum chamber onto the second expansion stage ("cold tip") of a 10 K closed cycle cryostat. Room temperature nH_2 gas enters the o/p converter through a 1.6 mm OD stainless steel (SS) tube, several windings of which are thermally anchored to the ≈ 50 K first expansion stage of the closed cycle cryostat. The same SS tube conducts the precooled nH_2 gas to the bobbin/tube assembly. Converting 50 K nH_2 gas to liquid pH_2 at 20 K releases about 2.3 kJ/mol [ref. 22]. The nominal cooling capacity of our cryostat is 2 W at 20 K, which limits nH_2 inlet flow rates to below about 3 mol/hour.

B. Deposition of Cryogenic Hydrogen Solids

As shown in figure 2, solid H_2 samples are prepared in a separate cryostat by deposition onto a 4 mm thick single crystal BaF_2 substrate clamped in a gold-plated OFHC copper holder cooled by a lHe bath cryostat (all thermal connections are made with 0.1 mm thick indium foil). The pre-cooled converted H_2 is delivered to the substrate through a thin wall brass tube oriented

at a 45° angle to the substrate surface normal; the tube terminates about 3 cm from the center of the sample substrate. The tube is supported near its open end by a room temperature polymer centering ring which makes only loose "knife edge" contact; we do not monitor the temperature of the brass tube, nor of the converted H_2 gas flow.

Because of the sample-in-vacuum design of our cryostat, sample thickness growth rates are limited to < 1 cm/hour by the pumping speed of the small turbomolecular pump which maintains the cryogenic thermal isolation vacuum ($P < 10^{-4}$ Torr uncondensed H_2 required to avoid thermal runaway). Ultimate sample thickness is limited by the 3 liter capacity of our lHe bath cryostat. The uncondensed H_2 also results in the deposition of a second solid H_2 film on the back side of the BaF_2 substrate, amounting to 8.7(±0.5)% of the main front side sample thickness; this front:back thickness ratio is independent of H_2 inlet flow rate.

IR absorption spectra of the solids are obtained with a Fourier transform infrared (FTIR) spectrometer capable of 0.1 cm^{-1} resolution, which simultaneously probes both front and back side H_2 samples. To accommodate the IR diagnostic, the cryostats reside inside a 0.5 m^3 polycarbonate box purged with a constant flow of dry N_2 gas.

C. Gas Phase Thermal Conductivity Apparatus

A popular technique for determining the ortho/para composition of a sample of H_2 gas is to measure its thermal conductivity (TC).[29] This approach exploits the large differences in rotational heat capacities (and hence in TCs) between the ortho and para H_2 species which occur in the 100 to 200 K region.[11] In our apparatus, this analysis method allows us to characterize the performance of our o/p converter by collecting gas samples at much higher H_2 gas flow rates than can be accommodated during a solid H_2 deposition. As typically implemented, this technique does not actually require the explicit calculation of absolute TCs; rather, unknown ortho/para compositions are extracted by comparison with a calibration curve made using H_2 samples of known composition.

We employ a variant of the transient hot wire technique in which the (absolute) TC of a dielectric medium surrounding a thin metal wire can be deduced from the time dependence of an electrically induced temperature jump (T-jump) in the wire.[30-34] We will not give a complete description of our implementation of this technique; we only document significant modifications

to the standard method.[31]

Ideally, the time dependent T-jump in a very thin wire is given by:[32]

$$\Delta T(t) = \frac{q}{4\pi\lambda} \ln\left(\frac{4\kappa t}{a^2 C}\right) \qquad (1)$$

in which: q is the electrically induced heat flux per unit length of wire, λ is the thermal conductivity of the surrounding dielectric medium, κ is the thermal diffusivity of the dielectric, a is the radius of the wire, and $C = \exp(\gamma)$ where γ is Euler's constant ($\gamma \approx 0.5772$). Thus, a plot of $\Delta T(t)$ vs. ln(t) should yield a straight line with slope $q/(4\pi\lambda)$. In practice, deviations occur for both short and long times following the T-jump. Under typical experimental conditions (q = 0.390 W/m) our plots are suitably linear for delays of between 20 and 100 ms after the T-jump.

Figure 3 shows a diagram of the TC cells and pressure vessel assembly. The bodies of our two TC cells are constructed of 17 mm ID copper tubing. The active element in each cell is a piece of 15 μm diameter tungsten wire suspended along the tube axis; the long-cell wire measures 22.3 cm, the short-cell wire 7.2 cm. The ends of these wires are held in crushed 1.6 mm OD copper tubes which are silver soldered to #6-32 brass machine screws. These screws extend through electrically insulating polymer caps which are press-fit into the ends of the cells. The tungsten wires are kept straight by weak tensioning springs bearing on adjustable hex-nuts. Each cell has two 6.4 mm diameter clear holes, one near each end, to admit the sample gas. Electrical connections are made with single strand copper wires insulated with loose fitting polymer sleeves.

The two cells fit inside a 38 mm ID copper tube pressure vessel, which is closed by a copper plated SS flange making a crushed indium wire seal. The cells' electrical wires, and the leads from a type-E (nickel-chromium vs. copper-nickel) thermocouple, feed through the top flange (not shown) and are sealed with a cryogenic compatible electrically insulating epoxy. Most of the thermocouple wire is insulated by polymer tubing sealed near the exposed junction with the same epoxy. The top flange also includes a valved inlet for the sample gas.

During a T-jump measurement the pressure vessel is oriented with its long axis vertical, and is completely submerged in a chilled liquid contained in a 20 liter SS dewar. Achieving a

constant temperature bath in the 100 to 200 K region is one of the more troublesome aspects of our TC experiment. The difference in rotational heat capacities between nH_2 and pH_2 reaches a maximum of 36% near 140 K, drops to 25% at 195 K, and to only 8% at 273 K; the sensitivity of the ortho/para determination via TC measurements is roughly proportional to this difference. We make our TC measurements at a temperature of 195 K, using an acetone bath chilled by a closed cycle refrigerator (supplemented by manual addition of small amounts of liquid nitrogen) and stirred by bubbling N_2 gas from the dewar bottom. With diligence, this approach results in measured temperature variations of less than ± 0.3 K during a typical experimental sequence.

Figure 4 shows an electrical schematic of our transient hot-wire TC experiment. The long and short cells are incorporated into a symmetrical Wheatstone bridge which can be balanced by adjusting the variable resistors. This circuit helps cancel unwanted end effects in the tungsten wire; the system behaves as if there were a 15.1 cm "unsupported" section of tungsten wire in the lower left arm of the bridge. The T-jump is induced in the tungsten wires by switching an electrical current from the dummy load resistor to the bridge. The temperature change causes a change in the electrical resistance of the tungsten wires which unbalances the bridge. In the standard method the bridge is dynamically readjusted during a measurement by a complicated electro-mechanical system.[31] We have replaced this hardware with a digital storage oscilloscope that captures directly the time dependence of V_{out}. This voltage is converted to wire resistance and then to wire temperature using standard DC circuit analysis (ignoring inductances and capacitances) and our in situ temperature calibrations.

III. RESULTS AND DISCUSSION

A. Infrared Absorptions of Cryogenic Hydrogen Solids

In our first MIS study utilizing the o/p converter,[35] we deposited the precooled pH_2 gas onto a 2 K substrate at conventional matrix host gas flow rates of ~ 1 mmol/hr. As expected from our experience with slow nH_2 depositions, these matrices exhibited significant optical scattering: a $\approx$ 50 μm thick pH_2 matrix showed scattering losses of $\approx$ 20 % at $\lambda = 2$ μm.

Figure 5 shows a portion of the IR absorption spectrum of a 4.5 mm thick pH_2 solid deposited at 290 mmol/hr; no wavelength dependent scattering losses were observed across the probed 1.5 to 6 μm region, and visual inspection confirmed the sample's excellent transparency.

Figure 6 shows IR absorption spectra of five solid H_2 samples deposited at ≈ 55 mmol/hr, of different oH_2 compositions obtained by adjusting the temperature of the o/p converter bobbin. Again, none of these samples exhibited appreciable optical scattering, either visually or in the form of a wavelength dependent scattering background across the probed 2 to 10 μm range.

In the solid phase, infrared activity in the homonuclear diatomic H_2 molecules arises from dipoles induced by intermolecular interactions with dopants and/or other host pH_2 molecules.[13-16] We consider first the IR activity induced by other pH_2 molecules (to establish the microscopic structure of our vapor deposited samples), and then return to the IR activity induced by dopants such as oH_2 molecules (to establish the ortho/para composition).

In pure solid pH_2, the IR absorption spectrum helps reveal the symmetries of the sites occupied by the pH_2 molecules. The absence of the $Q_1(0)$ line in figure 5 eliminates significant contributions from amorphous or porous structures;[36] however, any arrangement of close packed planes such as face centered cubic (fcc), hexagonal close packed (hcp), or random-stacked close packed (rcp) may be present. The presence of the $S_1(0)$ line in figure 5 requires that at least some pH_2 molecules reside in hcp or rcp regions, *i.e.* in sites which lack a center of inversion. The Raman scattering spectrum of this sample (ref. 27, figure 3c) shows a "quartet" pattern for the $S_0(0)$ transition, which reveals the as-deposited microscopic structure to be a mixture of hcp and fcc domains.[37] A "triplet" lineshape pattern is obtained by warming the sample to 4.5 K, matching the known Raman spectrum of hcp solid pH_2.[27, 37, 38]

The presence of oH_2 impurities in a close packed pH_2 solid reduces the symmetry of neighboring pH_2 molecules' environments, resulting in further distortions to their charge distributions. The dominant interaction is polarization of the nearest neighbor pH_2 molecules by the electric quadrupole of the oH_2 molecule.[14,15] In millimeters thick samples, oH_2 concentrations of just a few percent are sufficient to induce detectable IR activity in the $Q_1(0)$ and $Q_1(0)+S_0(1)$ bands, as shown in figure 6b. The observed spectral intensity changes with increasing oH_2 concentrations shown in figure 6 match quantitatively those reported for solid hydrogen crystals grown from the melt.[13]

The dependence of the $Q_1(0)$ band integrated intensity on the oH_2 and pH_2 fractions (F_o and F_p, respectively; $0 \le F \le 1$) is given by:[13]

$$(1/\ell) \int \log_{10}(I_0/I)\, d\bar{\nu} = a F_o^2 + b F_o F_p = b F_o + (a - b) F_o^2 \qquad (2)$$

where ℓ is the thickness of the sample. Thus, in the limit of low oH_2 concentrations, the $Q_1(0)$ band intensity is directly proportional to the oH_2 concentration. From our data in figure 6b we extract a value for the proportionality constant b in Eqn. (2) of: $b \approx 30$ cm^{-2} ($\bar{\nu}$ in cm^{-1} and ℓ in cm). This value of b can be used, in turn, to estimate the oH_2 concentration of the sample depicted in figure 5. From the inset to figure 5 we estimate the $Q_1(0)$ band integrated intensity to be ≈ 0.001 cm^{-1}; application of Eqn. (2) yields an oH_2 fraction of $F_o \approx 8 \times 10^{-5}$, consistent with the value of $F_o = 1.0 \times 10^{-4}$ predicted assuming complete equilibration within the 15 K converter bobbin.[11]

This result demonstrates the complete equilibration to nearly pure pH_2 at an o/p converter bobbin temperature of 15 K and a H_2 gas flow rate of 290 mmol/hr. The close agreement between the IR absorption spectra of our vapor deposited H_2 solids shown in figure 6, and the spectra of H_2 solids grown from the melt,[13] further supports our contention of complete equilibration in our o/p converter at all temperatures studied using these ~ 100 mmol/hr H_2 gas flow rates.

B. Gas Phase Thermal Conductivity Measurements

Before applying the gas phase TC technique to characterization of H_2 samples produced at higher gas flow rates, we evaluate the technique on "standard" samples produced at ~ 100 mmol/hr H_2 flow rates, for which the performance of our o/p converter has been demonstrated by the IR absorption technique. Figure 7 shows these results for samples produced at 70 to 170 mmol/hr flow rates. Three TC measurements were made on each sample; each data point represents the value derived from a waveform averaged over 16 T-jumps. The straight line is a least squares fit to our data; the slope is 3.84×10^{-4}, the standard deviation of the residuals is 1.5×10^{-3} W/m-K ($\approx 1\%$).

We estimate the magnitude of our systematic errors by comparison with literature absolute TCs of nH_2 [ref. 39] and pH_2 [ref. 40]; these sources list estimated total errors of $\pm$ 1% (unspecified) and $\pm$ 1.5% (3 σ level), respectively. Our straight line fit values for the nH_2 and

pH_2 composition samples differ from the accepted values by 2 and 3 %, respectively; the deviation for pure pH_2 is statistically significant with 95% confidence. Given the plethora of potential sources of systematic error, and our unrefined experimental implementation, we are pleased with this level of agreement.

The precision of our TC measurements (about ± 1%) is substantially better than their overall accuracy (about ± 3%). Thus, we do not attempt to determine the ortho/para compositions of H_2 samples produced at high flow rates directly from the absolute TC measurements. Rather, we continue the strategy of measuring the TCs of H_2 samples of known composition (produced at ~ 100 mmol/hr flow rates), and then looking for significant deviations in samples produced at higher flow rates.

Figure 8 shows our results for five pH_2 samples produced at flow rates between 100 and 1900 mmol/hr. Five TC measurements were made on each sample; each data point (open circles) represents the value derived from a waveform averaged over 16 T-jumps. The averaged TC values for each sample are shown as closed circles; the standard deviation of these five mean values is 1.15×10^{-3} W/m-K (0.7%) around a global mean value of 0.15815 W/m-K. The TC of the sample produced at the highest flow rate is $+1.8 \times 10^{-3}$ W/m-K (+1.1%) higher than the global mean. Application of Student's t-test indicates that this deviation is <u>not</u> statistically significant at the 95% level, and in any case is of the wrong sign to be attributed to incomplete equilibration to pH_2 in the o/p converter. Hence, assuming the straight line interpolation with pH_2 composition shown in figure 7, all five samples are pure pH_2 within a 5% error limit (95% confidence).

IV. SUMMARY AND CONCLUSIONS

We have presented in detail the construction and operation of our ortho/para hydrogen converter, which we use for precooling and equilibrating the ortho/para composition of a hydrogen gas flow. We have discovered that, in contrast with all previously reported experience with vapor deposited hydrogen solids, cryogenic solid hydrogen samples deposited using this device at flow rates of ~ 100 mmol/hr are remarkably transparent, independent of their ortho/para composition. This phenomenon permits characterization of their microscopic structures and ortho/para composition by infrared absorption spectroscopy. Deposition with the ortho/para converter bobbin held at 15 K and at a hydrogen flow rate of 290 mmol/hr resulted in a 4.5 mm

thick parahydrogen solid with a residual orthohydrogen content of less than 0.01%, consistent with complete equilibration within the o/p converter. Gas phase thermal conductivity measurements on samples produced at 20 K and at hydrogen flow rates up to 1.9 mol/hr yielded residual orthohydrogen contents of $0(^{+5}_{-0})$%, consistent with the value of 0.2% expected for complete equilibration.

The rapid vapor deposition sample preparation method permits the doping of cryogenic parahydrogen solids by co-deposition of species produced in any of the various dopant sources developed in previous matrix isolation spectroscopy efforts. The combination of this new sample preparation method and high resolution spectroscopic techniques promises a deeper and more quantitative understanding of the structure and dynamics of doped parahydrogen solids than has been achieved for doped rare gas matrices. The long transparent optical pathlengths, and the desirable properties of parahydrogen as a matrix host, make these systems very attractive for analytical applications.

ACKNOWLEDGEMENTS

We gratefully acknowledge helpful conversations early in this project with Prof. I.F. Silvera. We thank Ms. M.E. DeRose, Dr. J. Harper and Dr. J.A. Sheehy for critical readings of this manuscript.

REFERENCES

1. A.M. Bass and H.P. Broida, Formation and Trapping of Free Radicals (Academic Press, New York, 1960).
2. S. Cradock and A.J. Hinchcliffe, Matrix Isolation (Cambridge University Press, Cambridge, 1975).
3. M. Moskovits and G.A. Ozin, Cryochemistry (John Wiley & Sons, New York, 1976).
4. D.W. Ball, Z.H. Kafafi, L. Fredin, R.H. Hauge, and J.L. Margrave, A Bibliography of Matrix Isolation Spectroscopy 1954-1985 (Rice University Press, Houston, TX, 1988).
5. I.F. Silvera, Rev. Mod. Phys. **52**, 393 (1980).

6. M.E. Fajardo, S. Tam, T.L. Thompson, and M.E. Cordonnier, Chem. Phys. **189**, 351 (1994).

7. M.E. Fajardo, M. Macler, and S. Tam, "Progress Towards Deposition of Velocity Selected Aluminum Atoms into Cryogenic para-Hydrogen Matrices" in Proceedings of the High Energy Density Matter (HEDM) Contractors' Conference held 5-7 June 1996 in Boulder CO, ed. P.G. Carrick and N.T. Williams, PL-TR-96-3037 (Phillips Lab, Edwards AFB, CA, 1997).

8. D.P. Strommen, D.M. Gruen, and R.L. McBeth, J. Chem. Phys. **58**, 4028 (1973).

9. T. Miyazaki, H. Tsuruta, and K. Fueki, J. Phys. Chem. **87**, 1611 (1983).

10. T. Momose, M. Miki, M. Uchida, T. Shimizu, I. Yoshizawa, and T. Shida, J. Chem. Phys. **103**, 1400 (1995).

11. D.A. McQuarrie, Statistical Mechanics (Harper & Row, New York, 1976). Molecular H_2 exists in two forms: "para" (pH_2) with paired nuclear spins (I=0) and in even rotational states (J=0, 2, ...), or "ortho" (oH_2) with I=1 and odd J. The two forms interconvert very slowly in the absence of a catalyst. At room temperature, the equilibrium composition of nH_2 is very nearly the high temperature limit of 3:1 oH_2:pH_2. At liquid helium temperatures the equilibrium shifts almost completely to pH_2 in the J=0 state; however, metastable oH_2 (J=1) molecules can become incorporated into SMH samples.

12. T.J. Lee, J. Vac. Sci. Technol. **9**, 257 (1972).

13. H.P. Gush, W.F.J. Hare, E.J. Allin, and H.L. Welsh, Can. J. Phys. **38**, 176 (1960).

14. J. Van Kranendonk and G. Karl, Rev. Mod. Phys. **40**, 531 (1968).

15. J. Van Kranendonk, Solid Hydrogen (Plenum Press, New York, 1982).

16. M. Mengel, B.P. Winnewisser, and M. Winnewisser, J. Mol. Spec. **188**, 221 (1998).

17. K. Inoue, H. Kanzaki, and S. Suga, Solid State Comm. **30**, 627 (1979).

18. T. Oka, Annu. Rev. Phys. Chem. **44**, 299 (1993).

19. D.P. Weliky, T.J. Byers, K.E. Kerr, T. Momose, R.M. Dickson, and T. Oka, Appl. Phys. B **59**, 265 (1994).

20. T. Momose, M. Miki, T. Wakabayashi, T. Shida, M.C. Chan, S.S. Lee, and T. Oka, J. Chem. Phys. **107**, 7707 (1997).

21. T. Momose and T. Shida, Bull. Chem. Soc. Jpn. **71**, 1 (1998).
22. P.C. Souers, Hydrogen Properties for Fusion Energy (University of California Press, Berkeley, 1986).
23. N. Schwentner and V.A. Apkarian, Chem. Phys. Lett. **154**, 413 (1989).
24. W.G. Lawrence and V.A. Apkarian, J. Chem. Phys. **97**, 2224 (1992).
25. F. Legay, N. Legay-Sommaire, and V. Chandrasekharan, J. Phys. Chem. **94**, 8548 (1990).
26. F. Legay and N. Legay-Sommaire, J. Phys. Chem. **99**, 5277 (1995).
27. M.E. Fajardo and S. Tam, J. Chem. Phys. **108**, 4237 (1998).
28. A. Roth, Vacuum Sealing Techniques (Pergamon Press, Oxford, 1966).
29. A.T. Stewart and G.L. Squires, J. Sci. Instrum. **32**, 26 (1955).
30. J.W. Haarman, Physica **52**, 605 (1971).
31. J.J. DeGroot, J. Kestin, and H. Sookiazian, Physica **75**, 454 (1974).
32. J.J. Healy, J.J. DeGroot, and J. Kestin, Physica **82C**, 392 (1976).
33. J. Kestin, R. Paul, A.A. Clifford, and W.A. Wakeham, Physica **100A**, 349 (1980).
34. M.J. Assael, M. Dix, A. Lucas, and W.A. Wakeham, J. Chem. Soc. Faraday Trans. 1 **77**, 439 (1981).
35. S. Tam, M. Macler, and M.E. Fajardo, J. Chem. Phys. **106**, 8955 (1997).
36. J. Van Kranendonk and H.P. Gush, Phys. Lett. **1**, 22 (1962).
37. G.W. Collins, W.G. Unites, E.R. Mapoles, and T.P. Bernat, Phys. Rev. B **53**, 102 (1996).
38. S.S. Bhatnagar, E.J. Allin, and H.L. Welsh, Can. J. Phys. **40**, 9 (1962).
39. M.J. Assael, S. Mixafendi, and W.A. Wakeham, J. Phys. Chem. Ref. Data **15**, 1315 (1986).
40. H.M. Roder, J. Chem. Eng. Data **29**, 382 (1984).

FIGURE CAPTIONS

FIG. 1. Oxygen free high conductivity copper bobbin.

FIG. 2. Solid hydrogen deposition experimental diagram.

FIG. 3. Thermal conductivity cells and pressure vessel.

FIG. 4. Electrical schematic of transient hotwire experiment. The TTL control circuitry and the heating circuit do not share a common ground.

FIG. 5. IR absorption spectrum of a 4.5 mm thick vapor deposited pH_2 solid. The sample was produced using a pH_2 gas flow rate of 290 mmol/hr, resulting in a sample thickness growth rate of $\approx$ 75 μm/min. During deposition the substrate temperature rose from 2.1 to 3.3 K; the spectrum was taken at 2.4 K. The absence of the $Q_1(0)$ (4153 cm^{-1}) and $Q_1(0)+S_0(1)$ (4740 cm^{-1}) absorptions indicates a very low residual oH_2 concentration (< 0.01%). Resolution is 0.25 cm^{-1} FWHM.

FIG. 6. IR absorption spectra of $\approx$ 0.8 mm thick vapor deposited H_2 solids. The oH_2 concentrations increase from bottom to top in the sequence: (a) 0.01%, (b) 2%, (c) 8%, (d) 25%, and (e) 70%, estimated from the o/p converter bobbin temperatures of: (a) 15 K, (b) 28 K, (c) 37 K, (d) 52 K, and (e) 135 K. In each case $\approx$ 55(±3) mmol of hydrogen were deposited onto a 2 K substrate in a 1 hour period. The spectra are presented at 1 cm^{-1} FWHM resolution.

FIG. 7. Thermal conductivity of H_2 gas samples at 1 atm and 198.3(±0.2) K produced at various o/p converter temperatures. The pH_2 compositions are calculated as 25.1%, 37.6%, 50.0%, 62.6%, 74.8%, 87.7%, and 99.8% from the corresponding o/p converter bobbin temperatures of: 297 K, 103 K, 78 K, 63 K, 52 K, 41 K, and 20 K; the H_2 gas flow rates are: 70, 90, 90, 100, 110, 155, and 170 mmol/hr, respectively. The straight line is a least-squares fit to our data. The closed symbols show the literature thermal conductivities of nH_2 and pH_2 gas samples at 198.3 K and 1 atm, interpolated from data in: ref. 39 (circle), ref. 40 (triangle).

FIG. 8. Thermal conductivity of pH_2 gas samples at 1 atm and 198.7(±0.3) K produced at five different H_2 flow rates. The o/p converter bobbin temperature was maintained at 20 K yielding nominal pH_2 compositions of 99.8%. Five measurements were made on each sample, the 25 individual data are shown as open circles. The closed circles show the averaged TC values for each sample; the error bars show ± 1 σ limits calculated for each point. The horizontal line shows the overall mean TC value.

Figure 1

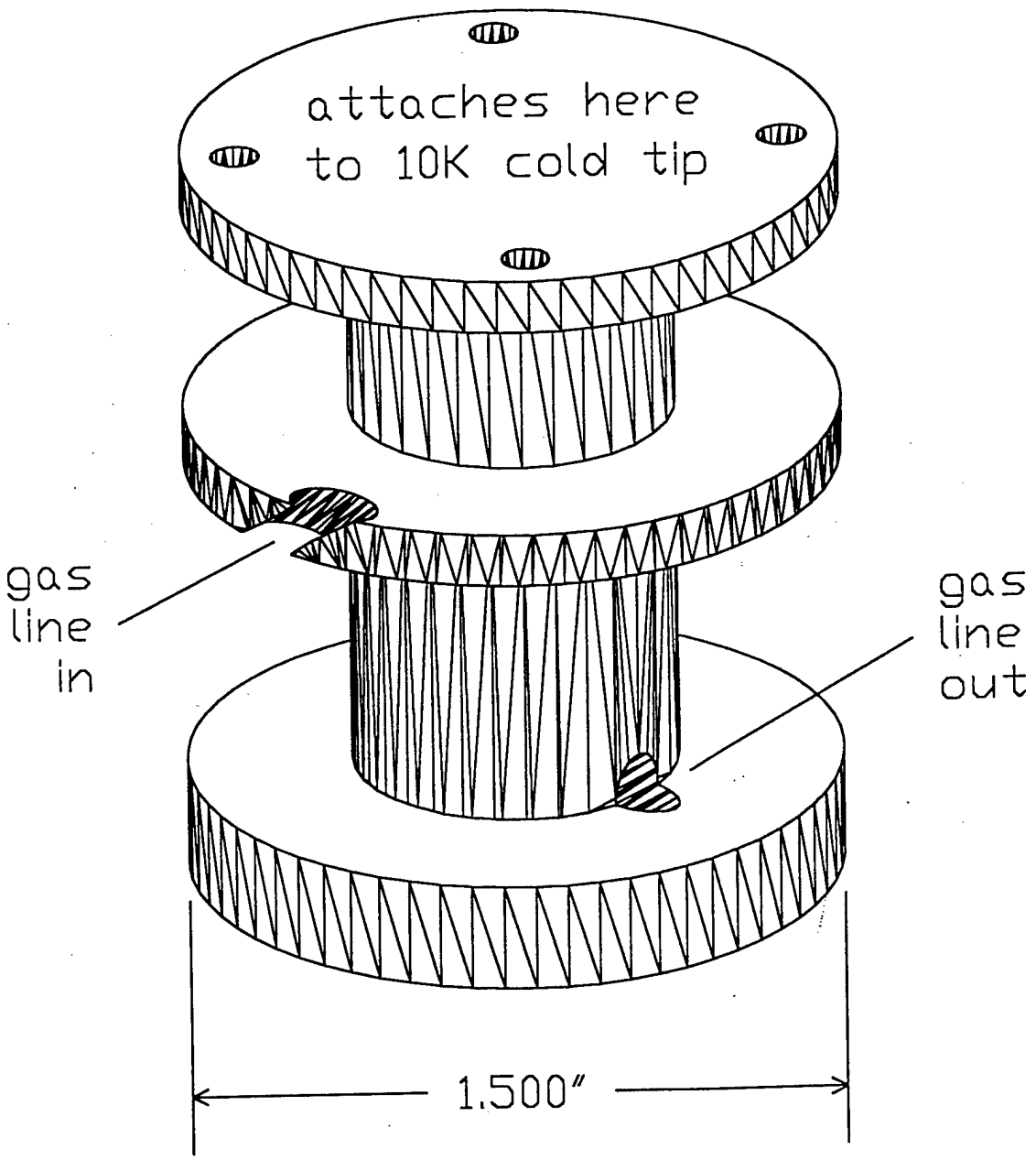

Figure 2

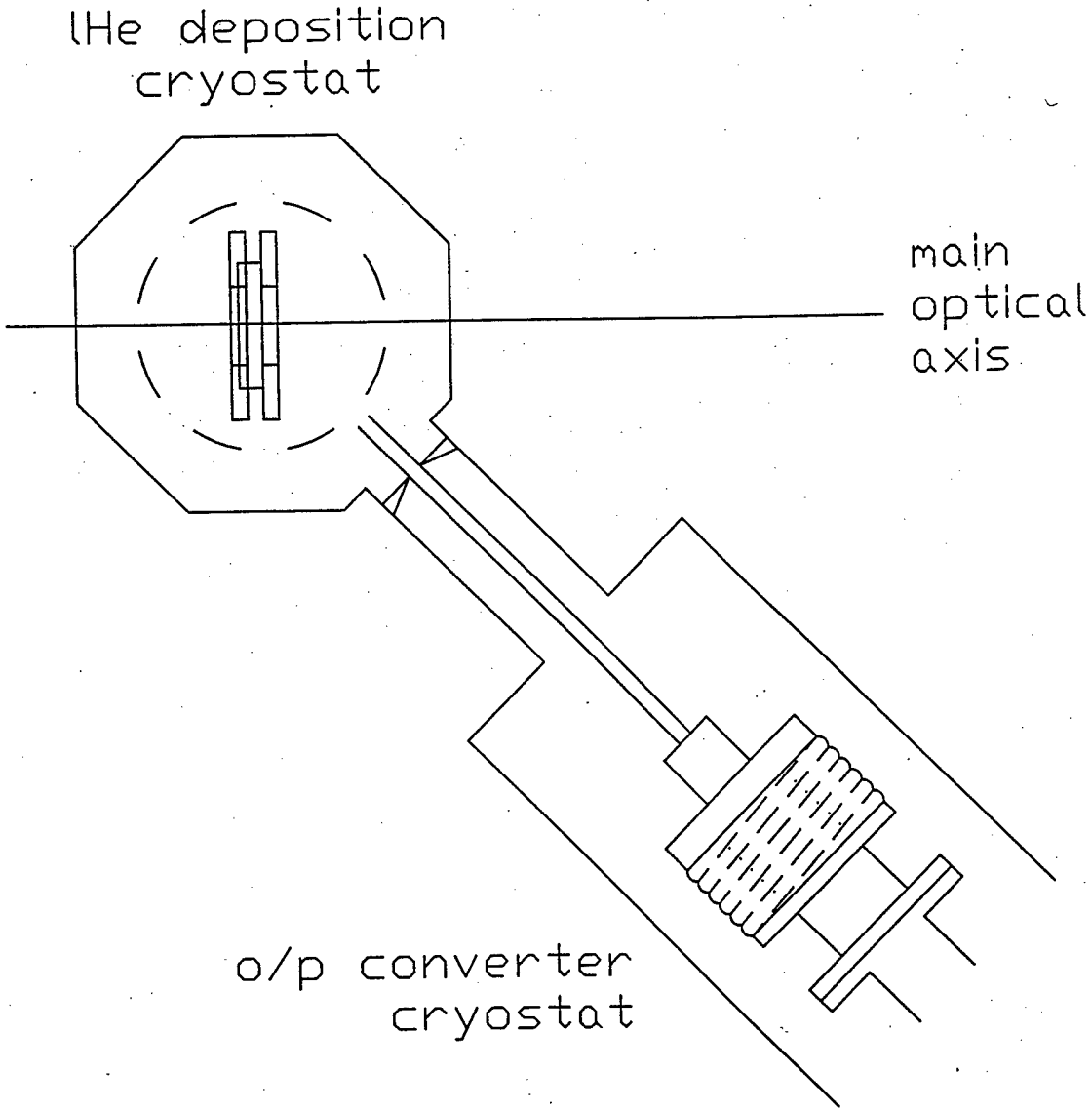
lHe deposition
cryostat
main
optical
axis
o/p converter
cryostat

Figure 3

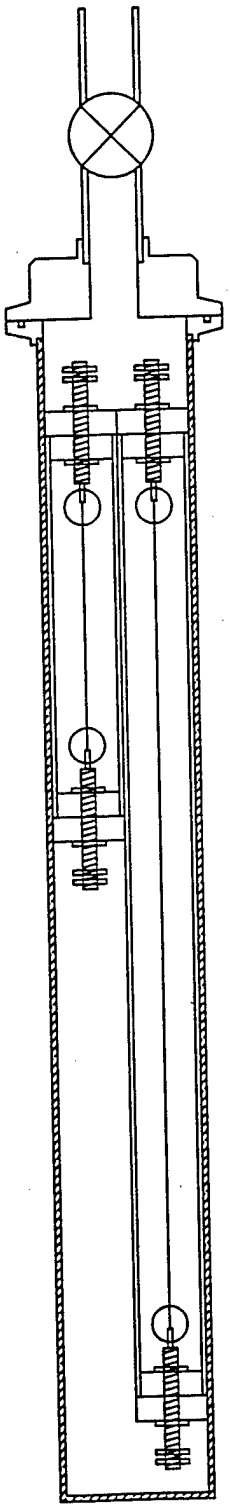

Figure 4

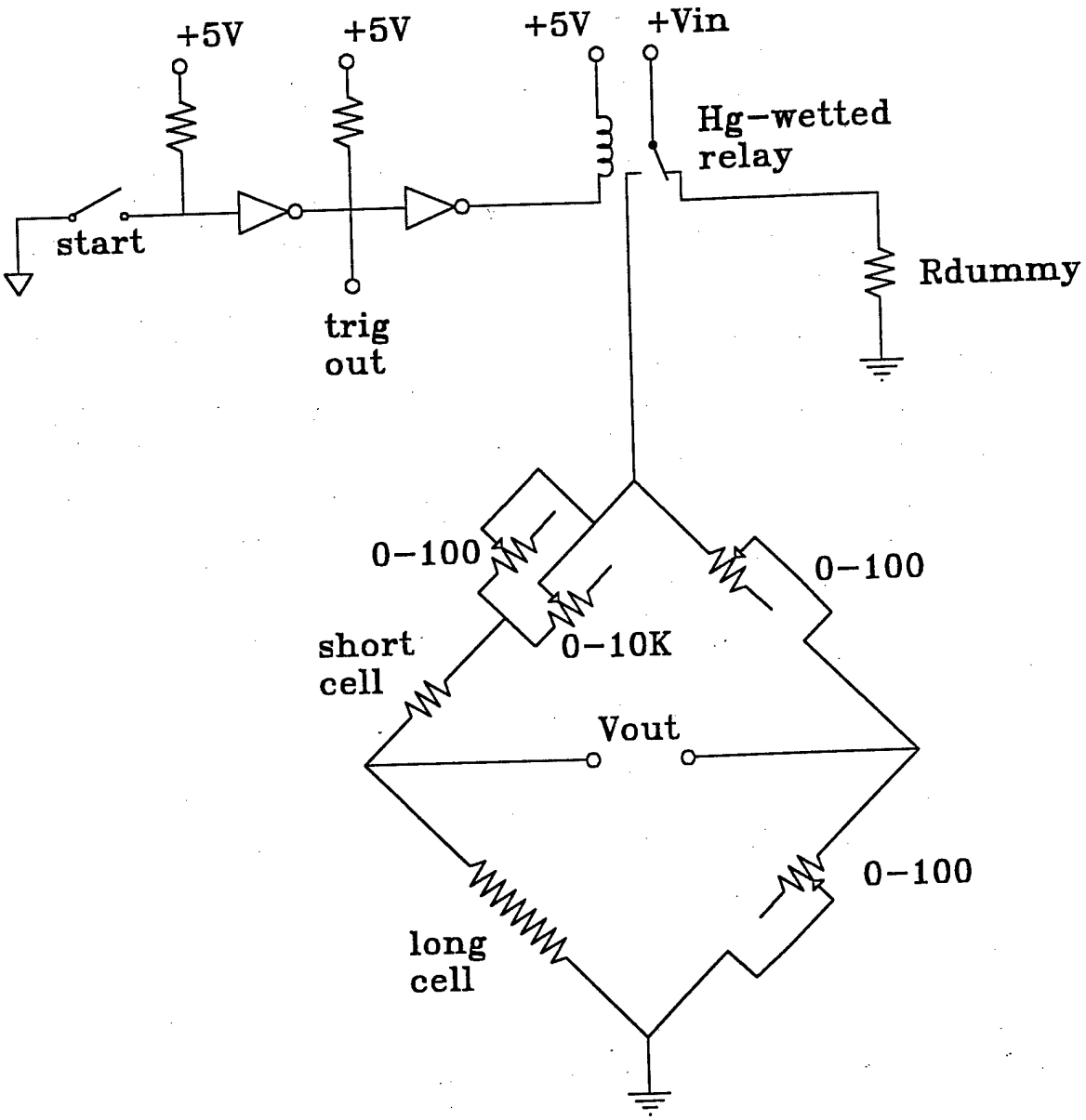
+5V
+5V
+5V
+Vin
Hg–wetted
relay
start
trig
out
Rdummy
0–100
0–10K
0–100
short
cell
Vout
0–100
long
cell

Figure 5

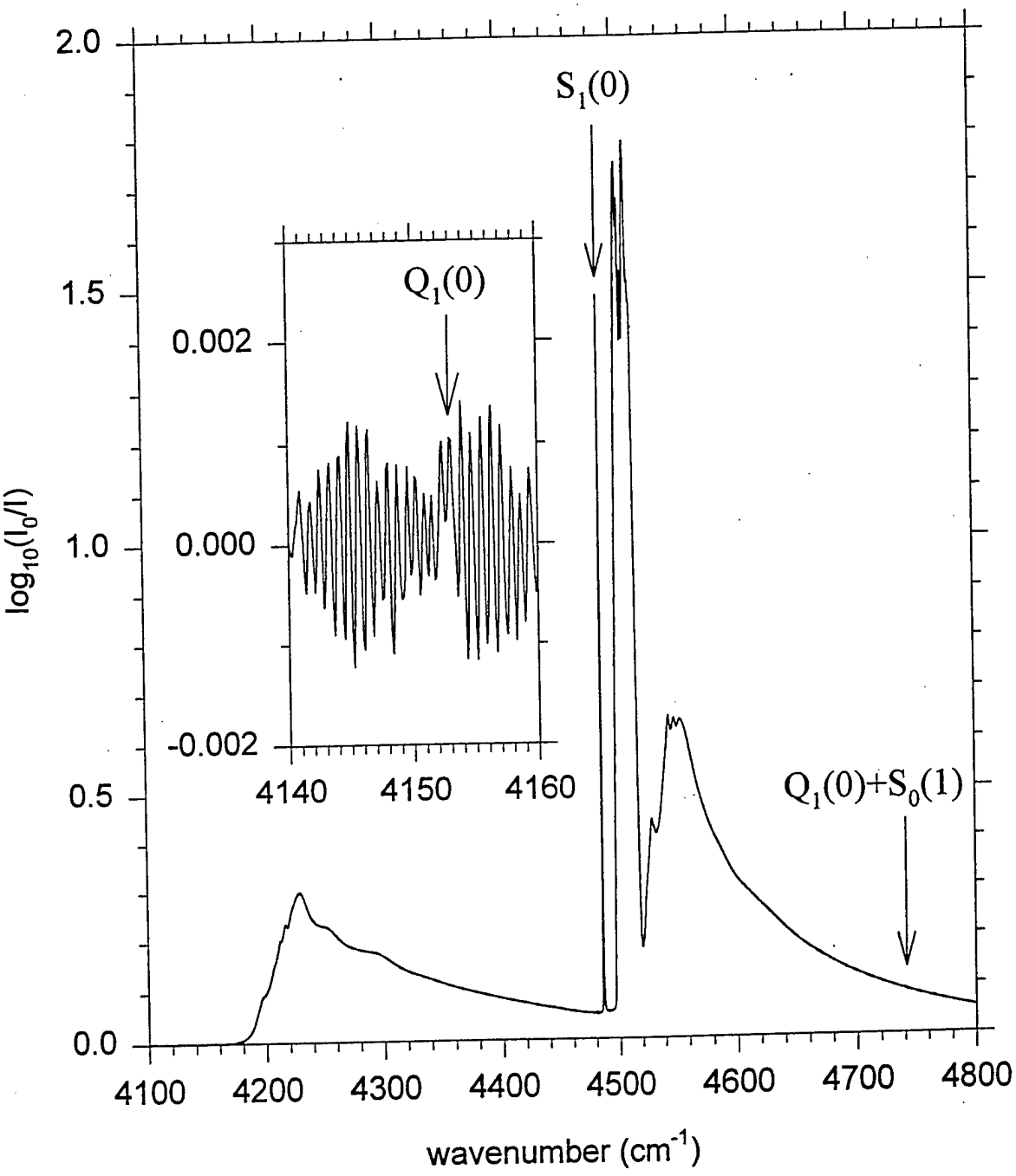

e:\pubnew\opconv\st2244a.spw

Figure 6

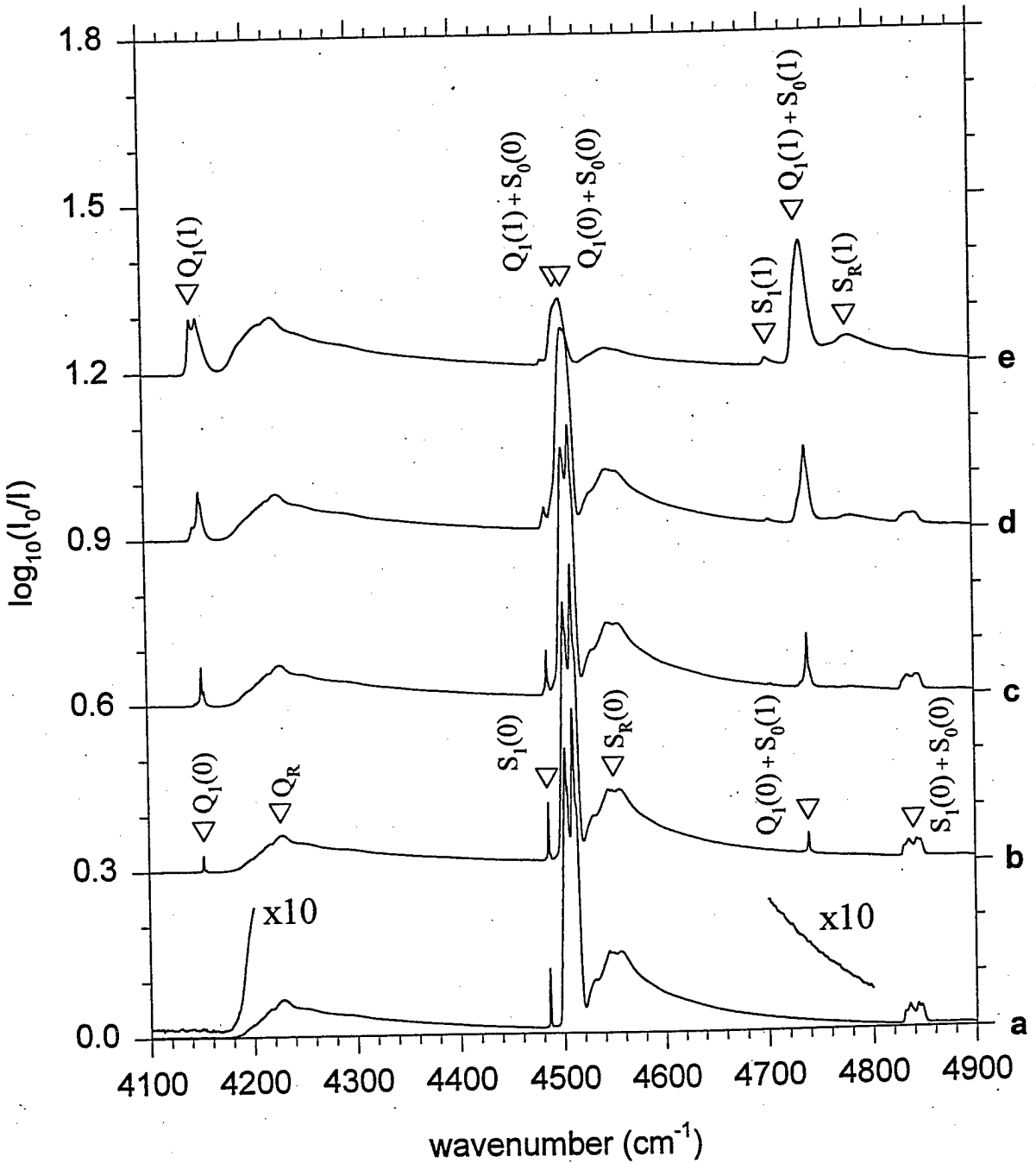

e:\pubnew\opconv\st18.jnb

Figure 7

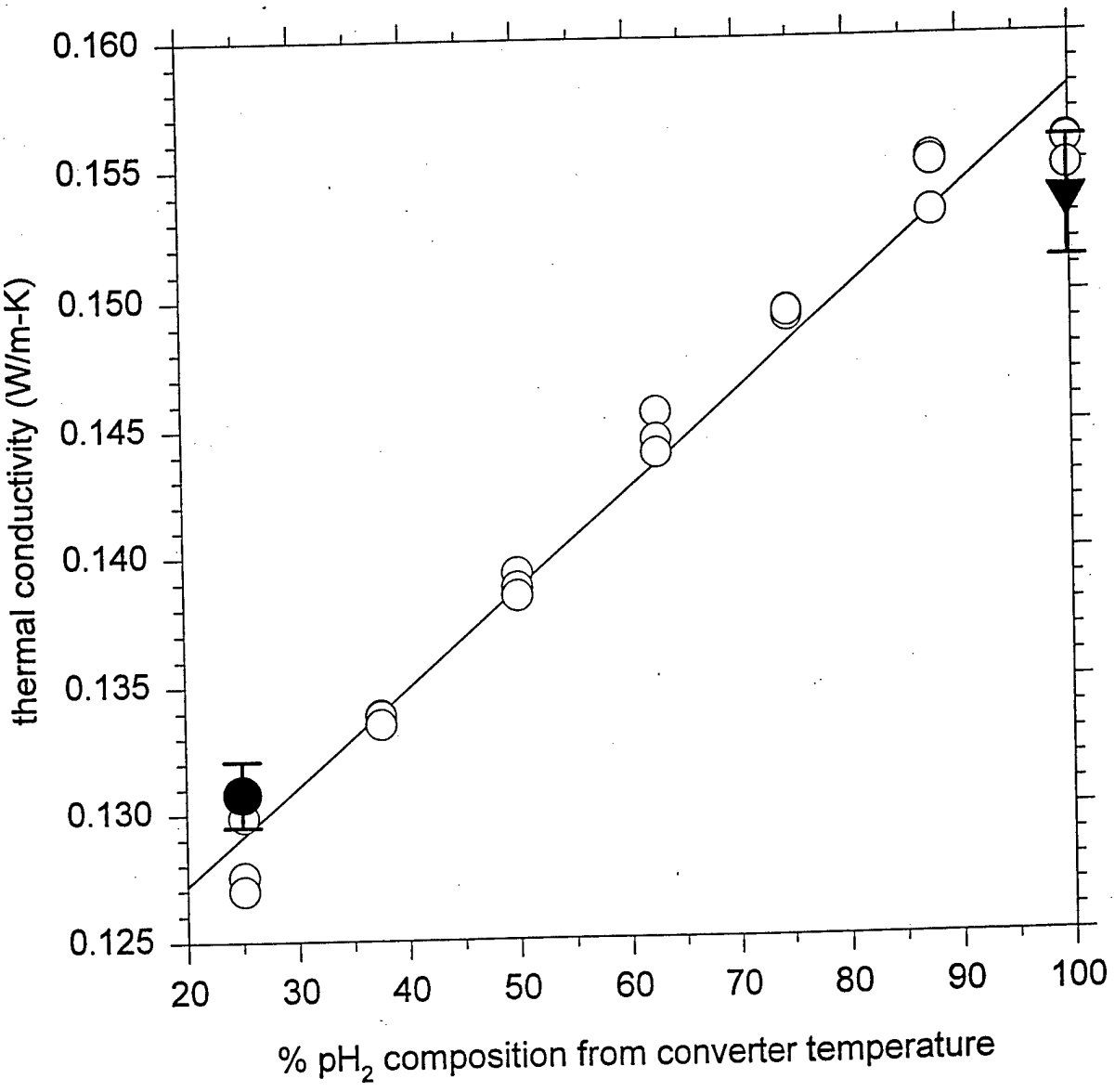

e:\pubnew\opconv\tc701.jnb

Figure 8

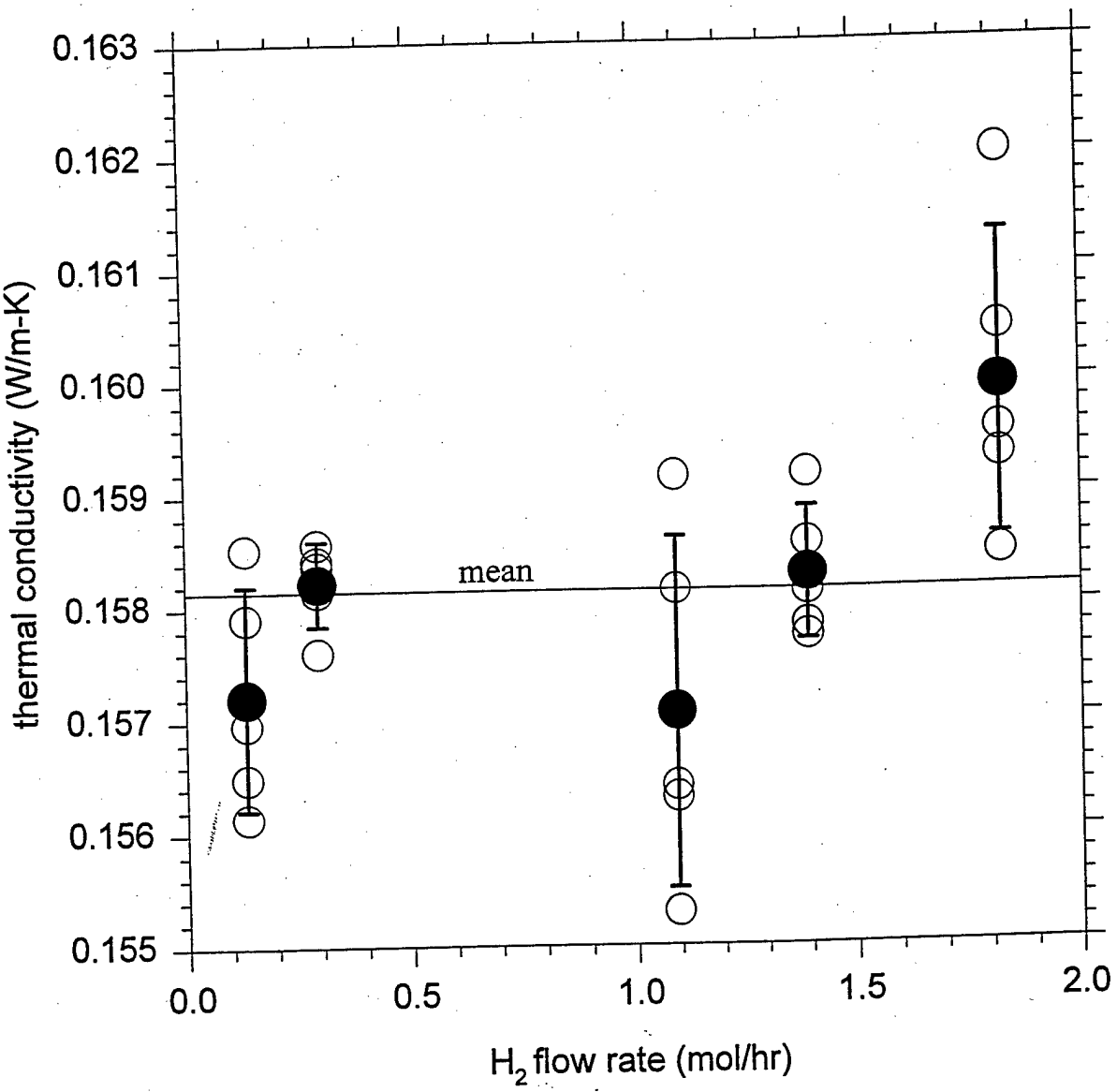

e:\pubnew\opconv\tc705.jnb